SMALL (1) 1017–1132 (2005) · ISSN 1613-6810
Volume 1 · No. 11 · November 2005

NANO MICRO

small

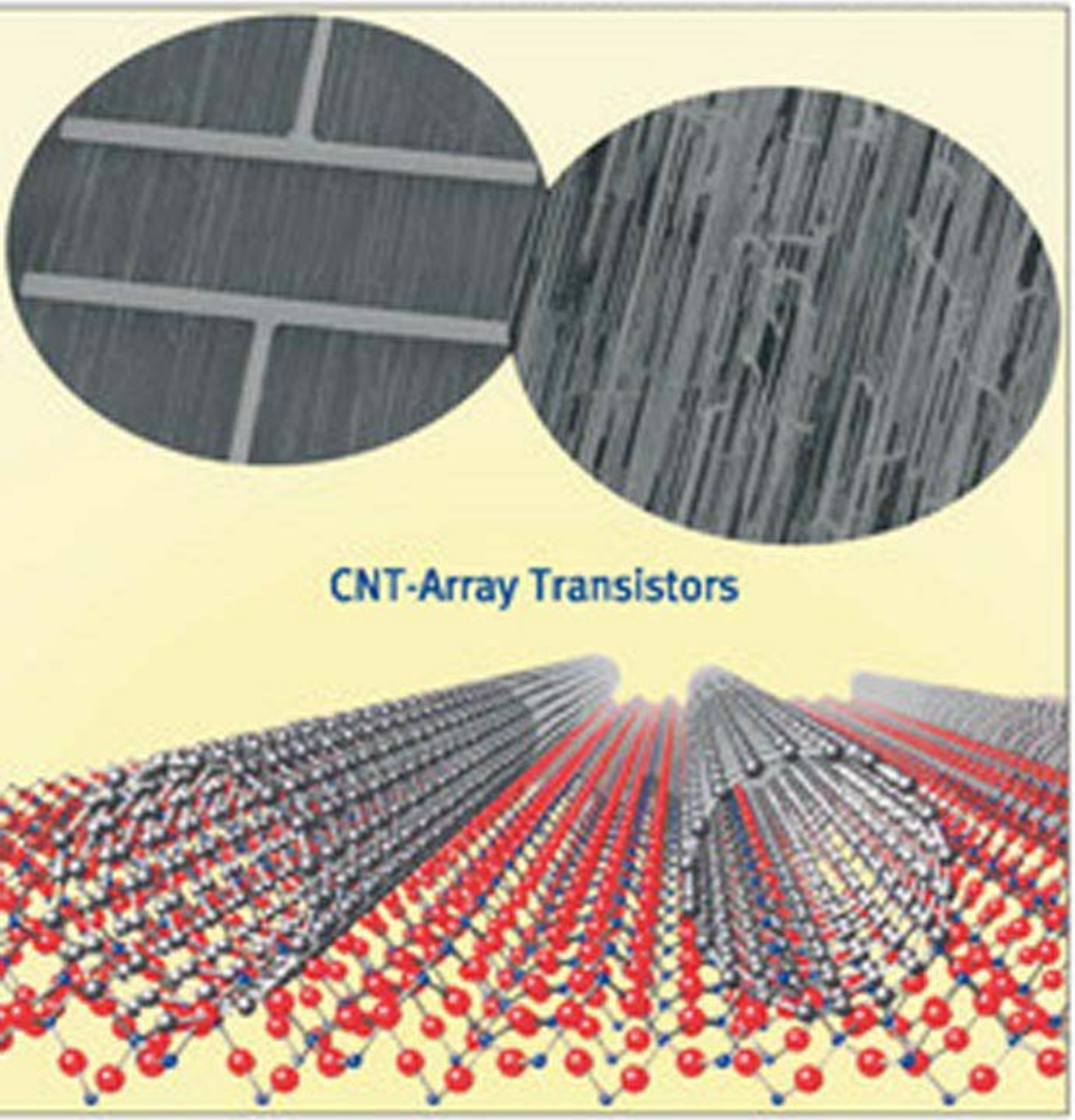

11/2005

Including contributions by:

John Rogers

Jillian Buriak

Reshef Tenne

Mauricio Terrones

Joseph Wang

WILEY-VCH

DOI: 10.1002/smll.200500120

Guided Growth of Large-Scale, Horizontally Aligned Arrays of Single-Walled Carbon Nanotubes and Their Use in Thin-Film Transistors

*Coskun Kocabas, Seung-Hyun Hur, Anshu Gaur, Matthew A. Meitl, Moonsub Shim, and John A. Rogers**

***A** convenient process for generating large-scale, horizontally aligned arrays of pristine, single-walled carbon nanotubes (SWNTs) is described. The approach uses guided growth, by chemical vapor deposition (CVD), of SWNTs on miscut single-crystal quartz substrates. Studies of the growth reveal important relationships between the density and alignment of the tubes, the CVD conditions, and the morphology of the quartz. Electrodes and dielectrics patterned on top of these arrays yield thin-film transistors that use the SWNTs as effective thin-film semiconductors. The ability to build high-performance devices of this type suggests significant promise for large-scale aligned arrays of SWNTs in electronics, sensors, and other applications.*

Keywords:
- nanostructures
- nanotechnology
- nanotubes
- surface chemistry
- transistors

1. Introduction

The high mobilities of single-walled carbon nanotubes (SWNTs) make them interesting for possible applications in nanoelectronics.[1–5] These electronic properties, together with the ability to deposit the tubes onto plastics and other unusual device substrates, make them also well-suited for use in large-scale distributed electronics for steerable antenna arrays, flexible displays, and other systems. Recent work indicates that random networks of SWNTs can form effective semiconductor layers for thin-film transistor- (TFT-) type devices.[6–11] The device mobilities that have been achieved with these networks are, however, still far below the intrinsic tube mobilities inferred from measurements of transistors that incorporate an individual tube (or small number of tubes) spanning the gap between the source and drain electrodes. The resistance at the many tube–tube contacts that are inherent in the networks may limit charge transport. Large-scale aligned arrays of SWNTs avoid this problem, thereby offering the possibility to exceed the device mobilities that can be achieved in the networks.

Some degree of alignment can be obtained by casting SWNTs from solution,[12–15] but dense arrays formed in this fashion usually involve large numbers of overlapping tubes. In addition, transistors that use solution-deposited tubes typically have properties that are inferior to those of transistors built with tubes grown directly on the device substrate by, for example, chemical vapor deposition (CVD). Arrays of SWNTs can be generated from random networks, formed

[*] C. Kocabas, Dr. S.-H. Hur, A. Gaur, M. A. Meitl, Prof. J. A. Rogers
Beckman Institute and
Frederick Seitz Materials Research Laboratory, Urbana, IL (USA)
Fax: (+1) 217-244-1190
E-mail: jrogers@uiuc.edu
C. Kocabas
Department of Physics
University of Illinois at Urbana/Champaign (USA)
Dr. S.-H. Hur, A. Gaur, M. A. Meitl, Prof. M. Shim, Prof. J. A. Rogers
Department of Materials Science and Engineering
University of Illinois at Urbana/Champaign (USA)
Prof. J. A. Rogers
Department of Electrical and Computer Engineering
University of Illinois at Urbana/Champaign (USA)
Prof. J. A. Rogers
Department of Chemistry
University of Illinois at Urbana/Champaign (USA)

NANO MICRO small

by CVD growth or solution deposition, via orientation-selective ablation with linearly polarized laser pulses.[16] This process has the advantage that it does not rely on chemistries or solvents that can alter the properties of the tubes; it is, however, an inherently destructive process. Electric-field-assisted growth[17,18] or fast heating[19] can produce aligned arrays of SWNTs. However, high-density arrays that cover large areas have not been demonstrated with these techniques; device implementations have also not been described. Recently, Ismach et al.[20] reported a new method of atomic-step-templated growth of aligned SWNTs on miscut sapphire crystals. Song et al.[21] reported directional growth of SWNTs on the a-plane and r-plane of a sapphire crystal, apparently unrelated to atomic steps. Herein, we show that large-scale, high-density, aligned arrays of SWNTs can be generated by guided CVD growth on standard low-cost, commercially available, single-crystal quartz substrates.[22] The nature of these arrays and the dependence of their characteristics (degree of alignment, tube diameter distribution, and coverage) on the growth conditions are described. These data suggest that the alignment mechanism on quartz may have some similarities to that on sapphire.[20] We also present the use of these large-scale arrays as effective semiconductor "thin films" for TFTs. The effective device mobilities (up to 125 $cm^2 V^{-1} s^{-1}$) are substantially higher than those that we have been able to achieve in random networks of SWNTs grown using similar techniques ($\approx 50\ cm^2 V^{-1} s^{-1}$).[5–10] The results indicate that low-cost quartz substrates can be used to generate high-quality aligned arrays of SWNTs for a range of applications in electronics and sensing.

2. Results and Discussion

Figure 1a shows atomic force microscope (AFM) images of SWNTs grown on SiO_2/Si using the procedures described in the Experimental Section. The random networks observed in this case are similar to those that we previously used in thin-film-type transistors.[10] The distributions of the tubes on quartz (Figure 1b) involve aligned arrays and few tube–tube crossings; they are very different to those observed on amorphous substrates, including SiO_2 and fused quartz. Figure 1c and d presents histograms of the tube orientations and diameters for the region of the substrate shown in Figure 1b, respectively. The AFM images are consistent with tubes that are mainly individual single-walled with diameter 1 ± 0.5 nm. The structures with diameters larger than 2 nm could be small bundles. The diameter distribution is similar to that of tubes grown on SiO_2/Si.

Figure 2a shows schematically a quartz crystal (trigonal symmetry) and the orientation of a Y-cut wafer. Most of the results illustrated herein use the AT cut, which is a type of rotated Y cut that has a cut angle of 35°15′. This type of wafer is often used in surface acoustic wave devices, microbalances, and resonators. We observed similar tube distributions on quartz with slightly different Y-cut angles such as 36 or 38°. Figure 2b shows a cross section of the quartz wafer and the $01\bar{1}$ atomic planes. The wafers have some

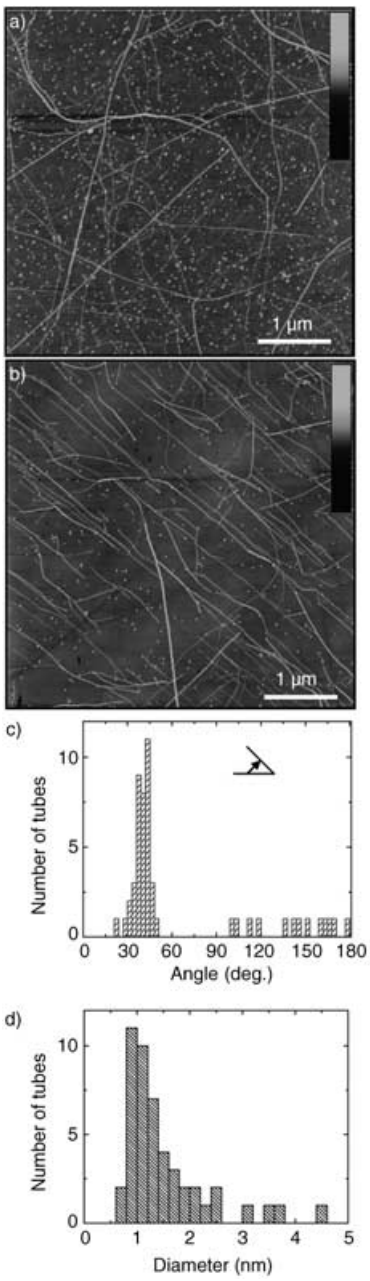

Figure 1. AFM images of random (a) and aligned (b) SWNTs grown on SiO_2 and single-crystal quartz, respectively. Histograms of the orientation (c) and diameter (d) of the aligned SWNTs. These data suggest that most of the aligned tubes are individual tubes. In (a, b) the color bar represents 10 nm height.

degree of miscut with respect to these planes. This miscut can lead to steps on the surface, as shown schematically in Figure 2c. These types of steps have been observed directly on other quartz planes.[23,24] It is likely that similar steps exist on the Y-cut wafers, although we are unaware of similar direct measurements of them. We did not observe these steps in AFM images of the as-received wafers due, possibly, to the small distances between them. Nevertheless, long thermal annealing (7 h, 900 °C) generated, in some cases, steps spaced sufficiently far apart to allow imaging by AFM (Figure 2d).

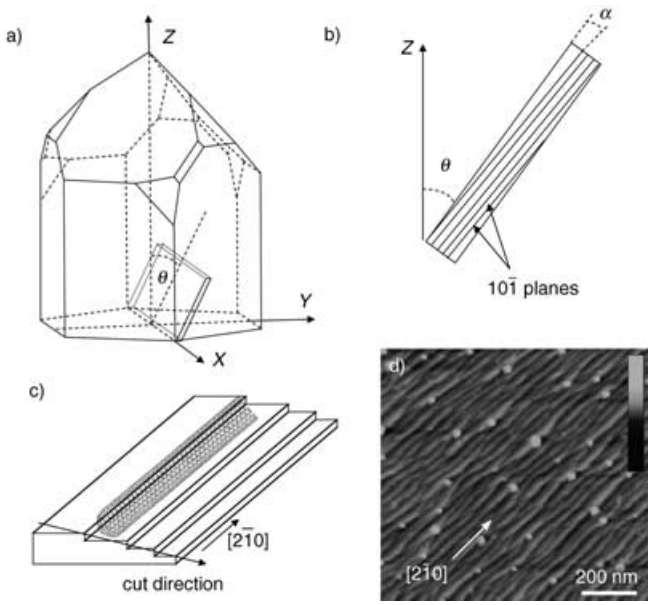

Figure 2. a) Schematic illustration of the crystallographic planes in right-handed α-quartz and the orientation of a Y-cut wafer. b) Cross section of an AT-cut quartz wafer and the 01$\bar{1}$ planes; the miscut angle is 2°58′. c) Schematic illustration of atomic steps and alignment direction on the surface. d) AFM image of terraced surface structures after thermal annealing. The steps in this case are 0.7–1-nm high with 30–35-nm spacing. The small particles are ferritin catalyst; the bar represents 5 nm height.

The alignment of tubes grown on these substrates is always parallel to the direction of the features in Figure 2d. It is independent of the direction of gas flow, for the growth conditions explored here. Figure 3a shows a collection of well-aligned tubes. The inset shows that the tubes are not perfectly straight; they have shapes that are similar to those observed in the step edges of Figure 2d. Figure 3a and b shows that the tubes also occasionally exhibit large, abrupt changes in their alignment. The shapes of these "kinks" are similar to those in step edges that are often observed in quartz and other single-crystal substrates such as Al_2O_3,[25] MgO,[26] and $MgAl_2O_4$[27] that have some small degree of miscut. Figure 3c presents an AFM image of aligned and unaligned SWNTs, and a scatter plot of orientation versus diameter appears in Figure 3d. Small-diameter tubes (<1.5 nm) are mainly aligned; as the tube diameter increases above this value, the degree of orientation decreases. The degree of alignment is also influenced by annealing of the quartz before tube growth. Figure 4a–c shows results obtained with substrates annealed at 900°C for 10 min, 4 h, and 7 h. Increasing the annealing time, which may increase the degree of order in the crystal lattice near the surface as well as the lengths and order of the steps,[23] improves the alignment.

To further characterize the aligned tubes, we measured the Raman spectra (micro-Raman setup) of individual tubes in the arrays. The spectrometer (Jobin–Yvon confocal) used a 100× microscope objective to focus a He–Ne excitation laser (632 nm wavelength; ≈1-μm spot size; 5×10^5 W cm^{-2} power density) and to collect the backscattered Raman signal through a 50-μm pinhole. Figure 5a shows the Raman spectrum of the tangential mode of a single SWNT for various orientations of the linear polarization direction of the excitation laser. The one-dimensional nature of carbon nanotubes gives rise to highly anisotropic optical properties.[16,28,29] Figure 5b shows the dependence of the Raman signal on orientation. The data are accurately described with an approximate $\cos^2\alpha$ functional form, where α is the angle between the polarization direction of incident light and the tube axis. The radial breathing mode (RBM) could not be measured because of the intense Raman signal from the single-crystal quartz substrate. The thin film consists of an aligned array of SWNTs and shows high optical anisotro-

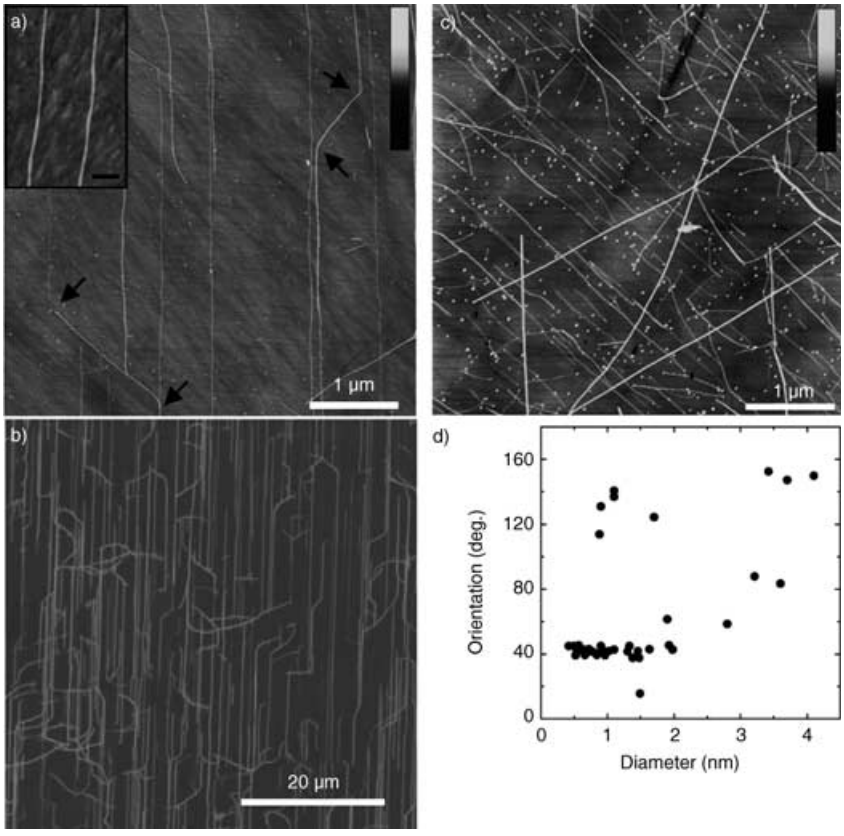

Figure 3. a) AFM image of SWNTs grown on single-crystal quartz substrates. The inset shows a high-magnification view of a pair of tubes (scale bar is 75 nm). Arrows in the main image highlight "kinks" in the tubes. b) Large-area SEM image of aligned tubes. c) AFM image of aligned and unaligned SWNTs. d) Scatter plot of the tube orientation versus the tube diameter. Large-diameter (>1.5 nm) tubes, which may be small bundles, are more likely to be unaligned than small-diameter (<1.5 nm) tubes. In (a–c) the color bar represents 10 nm height.

small NANO MICRO

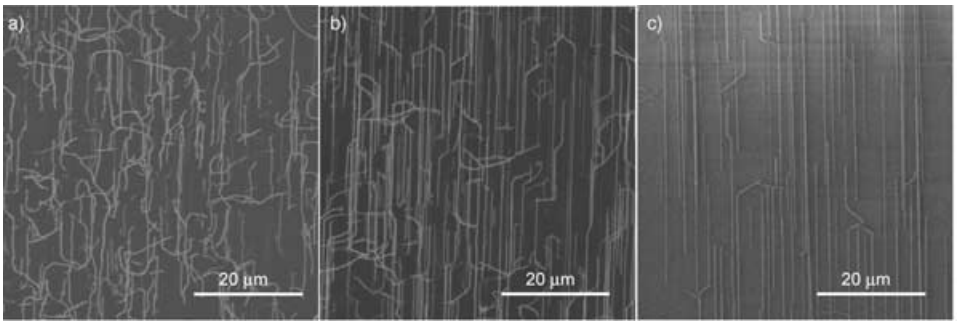

Figure 4. SEM images of SWNTs grown on quartz annealed at 900 °C for different times: a) 10 min, b) 4 h, c) 7 h.

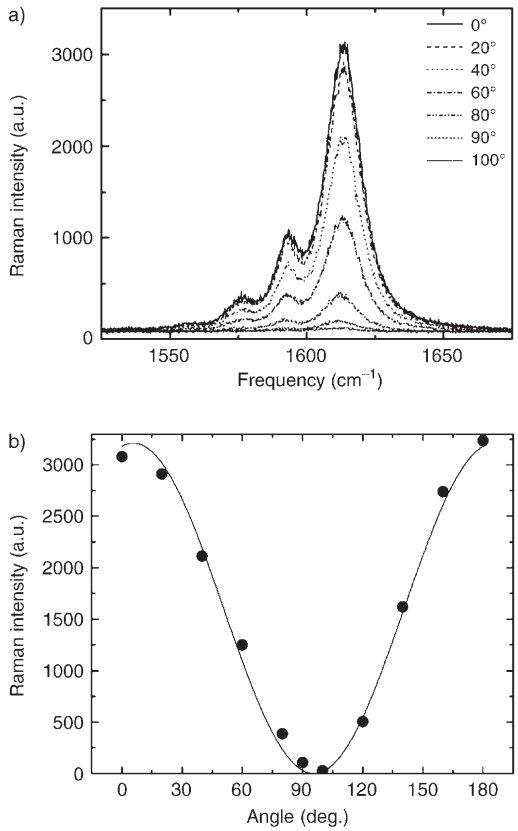

Figure 5. a) Raman spectrum of the tangential mode (G line) of an individual SWNT for various angles a between the polarization direction of the incident laser beam and the tube axis. b) Angular dependence of the Raman intensity at 1614 cm^{-1}. The solid line corresponds to a $\cos^2 a$ form. The Raman signal reaches a maximum when the laser beam is polarized along the tube.

py, which could find some application for optical devices.[30] In all other respects, the tubes on quartz have Raman signatures that are similar to those of tubes grown on SiO_2/Si. This spectroscopic information and the growth studies summarized in Figures 3 and 4 are consistent with an alignment mechanism that relies on energetically favorable van der Waals interactions of the tubes and/or catalyst particles with the SiO_2 lattice along certain crystallographic directions and/or with the step edges (or micro/nanofacets). Additional work is required to determine the details of the process.

High-performance TFTs and other devices benefit from closely packed, aligned arrays of SWNTs. The coverage can be controlled by changing the concentration of the catalyst particles. Figure 6a–c shows AFM images of SWNTs grown with different densities of catalyst particles (2000, 100, and 20 times dilution, respectively). With the growth conditions used here, there is a trade-off between coverage and alignment. In particular, the degree of alignment decreases with an increasing number of large tubes and bundles, both of which tend to form at high coverage. Figure 6d–f shows large areas imaged by SEM. For low densities (≈ 1 tube μm^{-1}), nearly perfect alignment can be achieved. The distributions of the lengths of the tubes appear as insets in Figure 6d and e. Generally, as the coverage increases, the average length of the tubes decreases. For the lowest densities, the average tube length can be ≈ 100 μm. Figure 7a–c shows SEM images for the highest coverage (> 10 tubes μm^{-1}) that we can currently achieve reliably. The large-area images illustrate the remarkable homogeneity of these aligned, submonolayer coatings of SWNTs.

To demonstrate one possible application of these arrays, we built TFTs by first fabricating source/drain contacts of Ti/Au (3- and 25-nm-thick) on the SWNTs by electron-beam evaporation followed by liftoff of a layer of photolithographically patterned resist (Shipley 1805). A layer of epoxy (SU-8; 1.6 μm thick) spin-cast and photopatterned on top of this structure formed a dielectric layer for a gate electrode (25-nm-thick Au) deposited by electron-beam evaporation through a shadow mask. Figure 8a and b shows SEM images of devices with channels aligned parallel and perpendicular to the direction of the aligned tubes. Figure 8c shows the transfer characteristics collected from devices similar to those shown in Figure 8a and b, but with much longer channel lengths (100 μm). The measurement results clearly show the expected anisotropic response. In the perpendicular configuration, the residual current is due to a small network effect generated by the small number of unaligned tubes. The effective device mobility is given by $\mu_d = \frac{\partial I_D}{\partial V_G}\frac{L}{WCV_D}$, where I_D is the drain current, V_G is the gate voltage, L is the channel length, W is the channel width, and V_D is the drain voltage. We estimate the gate capacitance C to be 2.3×10^{-5} F m^{-2} from the relation $C = \frac{\varepsilon\varepsilon_0}{t}$, where ε is the dielectric constant of the gate dielectric SU-8 (4.0), ε_0 is the vacuum permittivity, and t is the thickness of the gate dielectric. For the parallel configuration, the device mobilities (evaluated in the linear regime using standard procedures) can reach ≈ 125 cm^2 V^{-1} s^{-1} at channel lengths of 10 μm. This value is obtained with aligned SWNT arrays that have ≈ 10 tubes μm^{-1}. A simple geometrical calculation yields a

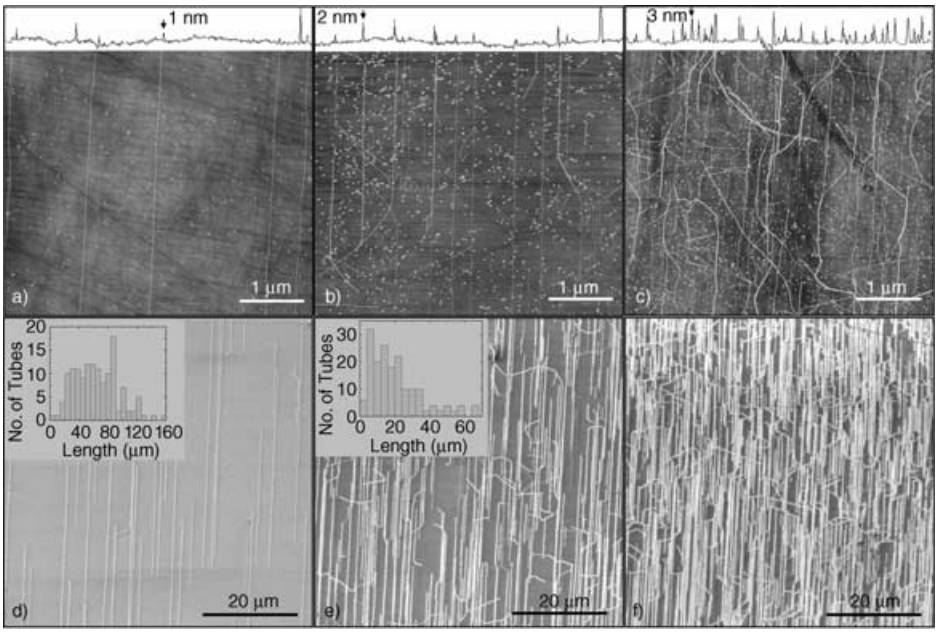

Figure 6. a–c) AFM images of aligned SWNTs grown on single-crystal quartz substrates using different densities of catalyst particles. d–f) Large-area SEM images of tubes grown in this fashion. These results indicate a decreasing degree of alignment with increasing tube density.

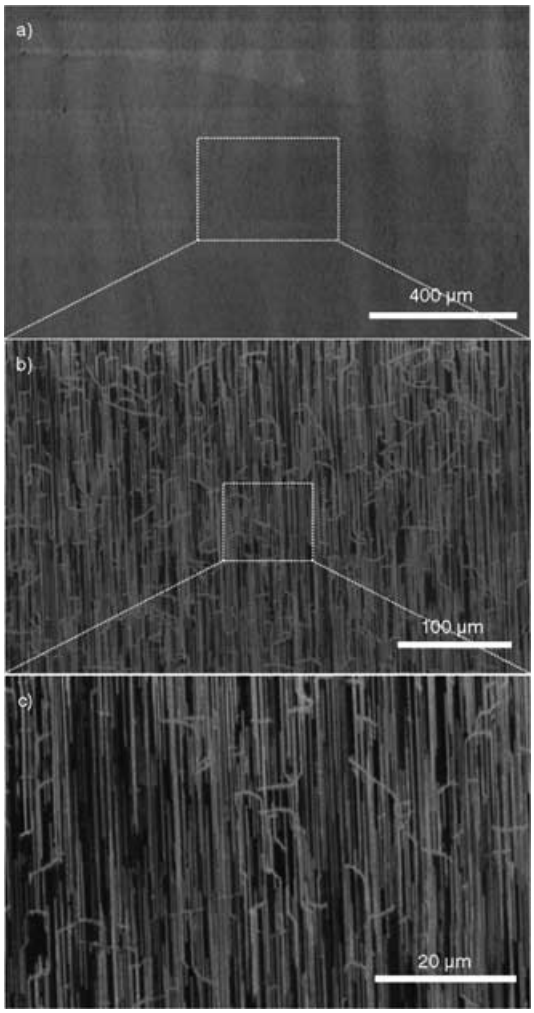

Figure 7. a–c) SEM images of high-density aligned tubes at different magnifications. These images show that aligned SWNTs are homogeneous over large areas.

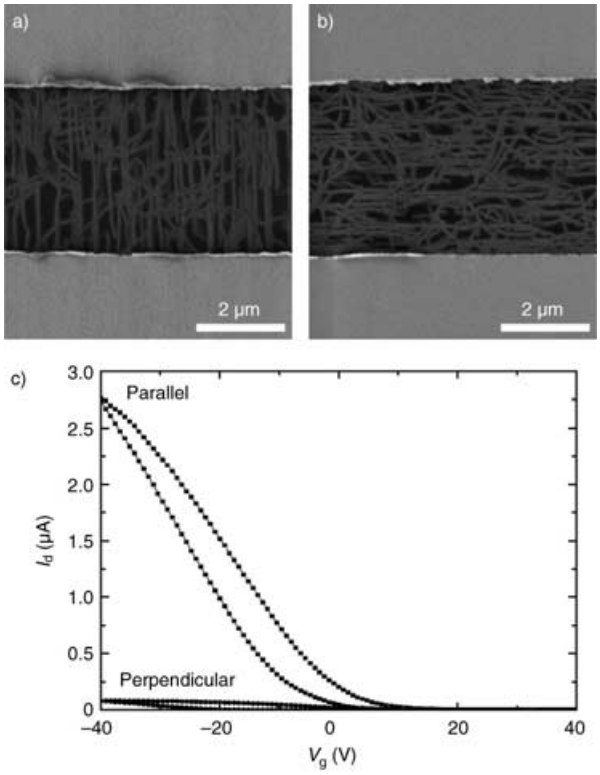

Figure 8. a, b) SEM images of channel regions of TFT devices that have their channels (5-μm channel lengths) aligned parallel and perpendicular to the orientation of the aligned SWNTs, respectively. c) Current–voltage response of TFTs with 100-μm channel length and 250-μm channel width, oriented parallel and perpendicular to the direction of alignment in arrays of SWNTs. The bias voltage V_D is 0.5 V. The aligned SWNTs behave like a highly anisotropic thin film. Device mobilities as high as 125 cm^2Vs^{-1}, corresponding to "per tube" mobilities of $\approx$9000 cm^2Vs^{-1}, can be observed in devices of this type.

small NANO MICRO

"per tube" mobility of $\approx 9000\ cm^2 V^{-1} s^{-1}$, which is comparable to that often observed in pristine single-tube devices. It is possible that increases in the coverage of the aligned SWNT arrays will lead to improved device mobilities. Achieving this goal is a central focus of our current work. (We note that short channel lengths yield low on/off ratios, due to the presence of metallic SWNTs that span the source/drain gap. These tubes can be selectively eliminated through electrical breakdown or chemical functionalization.[10,31])

3. Conclusions

In summary, we have shown that Y-cut single-crystal quartz can be used to generate well-aligned, densely packed, horizontal arrays of pristine SWNTs over large areas. Although additional work is required to understand more fully the detailed growth mechanisms, many of the features of the arrays and their dependence on growth conditions are consistent with either alignment along step edges or micro/nanofacets on the surface of the quartz or preferential interactions along certain directions associated with the quartz lattice. A step-edge alignment process recently described for miscut α-Al_2O_3[19] and a preferred interaction process for α-Al_2O_3 without miscut[20] may both be related to the observed effects. The low cost and commercial availability of Y-cut quartz and the ability to grow dense arrays of tubes represent attractive features of the approach introduced here. The format of these arrays (i.e., lying horizontally on a flat substrate) allows easy integration into devices, as demonstrated by high-performance TFTs. We believe that these types of arrays and the means for growing them will be valuable for a range of emerging applications that use large collections of SWNTs.

4. Experimental Section

Conventional CVD growth procedures are most well-established for use with SiO_2/Si substrates. Tubes were grown on this type of substrate to serve as a comparison for results on AT-cut quartz.[22] Ferritin catalyst (Aldrich) diluted 1:200 (v/v) with deionized water was cast onto the substrate, followed by heating at 900 °C for 10 min to oxidize the catalyst and cooling to room temperature. Heating to 900 °C in a hydrogen environment reduced the catalyst. Purging with hydrogen at 900 °C for 1 min and then introducing a flow of methane (2500 standard cubic centimeters per minute (sccm)) and hydrogen (75 sccm) at 900 °C for 10 min led to the growth of SWNTs. The quartz substrates were placed on polished Si wafers in the growth chamber to enhance the homogeneity of the temperature distribution on their surfaces. After growth, the samples were cooled slowly ($< 5\ °C\ min^{-1}$) to avoid cracking in the quartz.

Acknowledgements

We thank Prof. J. W. Lyding for the use of his AFM. This work was supported by the DARPA-funded AFRL-managed Macroelectronics Program (FA-8650-04-C-7101), the U.S. Department of Energy under grant DEFG02-91-ER45439, the NSF through grant NIRT-0403489, and a graduate fellowship from the Fannie and John Hertz Foundation (M.A.M.). AFM experiments were carried out in the Center for Microanalysis of Materials, University of Illinois, which is supported by the U.S. Department of Energy under grant DEFG02-91-ER45439.

[1] A. Javey, J. Guo, Q. Wang, M. Lundstrom, H. J. Dai, *Nature* **2003**, *424*, 654–657.
[2] S. Rosenblatt, Y. Yaish, J. Park, J. Gore, V. Sazonova, P. L. McEuen, *Nano Lett.* **2002**, *2*, 869–872.
[3] A. Javey, H. Kim, M. Brink, Q. Wang, A. Ural, J. Guo, P. McIntyre, P. L. McEuen, M. Lundstrom, H. Dai, *Nat. Mater.* **2002**, *1*, 241–246.
[4] A. Javey, R. Tu, D. B. Farmer, J. Guo, R. G. Gordon, H. Dai, *Nano Lett.* **2005**, *5*, 345–348.
[5] T. Durkop, S. A. Getty, E. Cobas, M. S. Fuhrer, *Nano Lett.* **2004**, *4*, 35–39.
[6] E. S. Snow, J. P. Novak, P. M. Campbell, D. Park, *Appl. Phys. Lett.* **2003**, *82*, 2145–2147.
[7] K. Xiao, Y. Liu, P. Hu, G. Yu, X. Wang, D. Zhu, *Appl. Phys. Lett.* **2003**, *83*, 150–152.
[8] K. Bradley, J. C. P. Gabriel, G. Grüner, *Nano Lett.* **2003**, *3*, 1353–1355.
[9] R. Seidel, A. P. Graham, E. Unger, G. S. Duesberg, M. Liebau, W. Steinhoegl, F. Kreupl, W. Hoenlein, *Nano Lett.* **2004**, *4*, 831–834.
[10] Y. Zhou, A. Gaur, S.-H. Hur, C. Kocabas, M. A. Meitl, M. Shim, J. A. Rogers, *Nano Lett.* **2004**, *4*, 2031–2035.
[11] E. S. Snow, P. M. Campbell, M. G. Ancona, J. P. Novak, *Appl. Phys. Lett.* **2005**, *86*, 0331051–0331053.
[12] M. A. Meitl, Y. Zhou, A. Gaur, S. Jeon, M. L. Usrey, M. S. Strano, J. A. Rogers, *Nano Lett.* **2004**, *4*, 1643–1647.
[13] M. D. Lay, J. P. Novak, E. S Snow, *Nano Lett.* **2004**, *4*, 603–606.
[14] S. G. Rao, L. Huang, W. Setyawan, S. H. Hong, *Nature* **2003**, *425*, 36–37.
[15] J. Liu, M. J. Casavant, M. Cox, D. A. Walters, P. Boul, W. Lu, A. J. Rimberg, K. A. Smith, D. T. Colbert, R. E. Smalley, *Chem. Phys. Lett.* **1999**, *303*, 125–129.
[16] C. Kocabas, M. A. Meitl, A. Gaur, M. Shim, J. A. Rogers, *Nano Lett.* **2004**, *4*, 2421–2426.
[17] Y. Zhang, A. Chang, J. Cao, Q. Wang, W. Kim, Y. Li, N. Morris, E. Yenilmez, J. Kong, H. Dai, *Appl. Phys. Lett.* **2001**, *79*, 3155–3157.
[18] E. Joselevich, C. M. Lieber, *Nano Lett.* **2002**, *2*, 1137–1141.
[19] S. Huang, X. Cai, J. Liu, *J. Am. Chem. Soc.* **2003**, *125*, 5636–5637.
[20] A. Ismach, L. Segev, E. Wachtel, E. Joselevich, *Angew. Chem.* **2004**, *116*, 6266–6269; *Angew. Chem. Int. Ed.* **2004**, *43*, 6140–6143.
[21] S. Han, X. Liu, C. Zhou, *J. Am. Chem. Soc.* **2005**, *127*, 5294–5295.
[22] The Roditi International Corporation Ltd.
[23] M. L. Schlegel, K. L. Nagy, P. Fenter, N. C. Sturchio, *Geochim. Cosmochim. Acta* **2002**, *66*, 3037–3054.
[24] A. J. Gratz, S. Manne, P. K. Hansma, *Science* **1991**, *251*, 1343–1346.
[25] J. R. Heffelfinger, M. W. Bench, C. B. Carter, *Surf. Sci.* **1997**, *370*, L168–L172.

[26] K. Sangwal, F. Sanz, J. Servat, P. Gorostiza, *Surf. Sci.* **1997**, *383*, 78 – 87.
[27] S. V. Yanina, C. B. Carter, *Surf. Sci.* **2002**, *512*, L402 – L412.
[28] G. S. Duesberg, I. Loa, M. Burghard, K. Syassen, S. Roth, *Phys. Rev. Lett.* **2000**, *85*, 5436 – 5439.
[29] Y. Murakami, E. Einarsson, T. Edamura, S. Maruyama, *Phys. Rev. Lett.* **2005**, *94*, 0874021 – 0874024.
[30] A. Star, Y. Lu, K. Bradley, G. Grüner, *Nano Lett.* **2004**, *4*, 1587 – 1591.
[31] C. Wang, Q. Cao, T. Ozel, A. Gaur, J. A. Rogers, M. Shim, *J. Am. Chem. Soc.*, in press.

Received: April 12, 2005
Published online on August 18, 2005

